JOURNAL OF MATERIALS SCIENCE 30 (1995) 201–211

Self-diffusion in α-Al_2O_3 and growth rate of alumina scales formed by oxidation: effect of Y_2O_3 doping

M. LE GALL, A. M. HUNTZ, B. LESAGE
Laboratoire de Métallurgie Structurale, CNRS, URA 1107, Bat. 413, Université Paris-XI, F-91405 Orsay Cedex, France

C. MONTY
Laboratoire de Physique des Matériaux, CNRS, 1 place Aristide Briand, F-92195 Meudon, France

J. BERNARDINI
Laboratoire de Métallurgie, CNRS URA 443, Université Aix-Marseille 3, F 13397 Marseille Cedex 20, France

In many cases, alumina scales are assumed to grow predominantly by oxygen diffusion, but some authors have found that the growth can be controlled by aluminium diffusion. These mechanisms can be modified by active elements. The problem with alumina is that there is a lack of data about self-diffusion coefficients, and, due to the stoichiometry of alumina, diffusion data correspond to an extrinsic diffusion mechanism so that it is not possible to compare oxygen and aluminium diffusion coefficients. In order to obtain information about the alumina scale growth mechanism, oxygen (^{18}O) and aluminium (^{26}Al) self-diffusion coefficients in Al_2O_3 were determined in the same materials and in the same experimental conditions, thus allowing a direct comparison. For both isotopes, bulk and sub-boundary diffusion coefficients were determined in single crystals of undoped alumina. Grain-boundary diffusion coefficients have been computed only for oxygen diffusion in polycrystals. Oxygen diffusion has been also studied for yttria-doped α-alumina in the lattice, sub-boundaries and grain boundaries. Oxygen and aluminium bulk diffusion coefficients are of the same order of magnitude. In the sub-boundaries, aluminium diffusion is slightly faster than oxygen diffusion. Yttria doping induces a slight increase of the oxygen bulk diffusion, but decreases the grain-boundary diffusion coefficients on account of segregation phenomena. These results are compared with the oxidation constants of alumina former alloys (alloys which develop an alumina scale by oxidation). It appears that neither lattice self-diffusion nor grain boundary self-diffusion can explain the growth rate of alumina scales. Such a situation is compared to the case of Cr_2O_3.

1. Introduction

Alumina is a structural ceramic of great technological interest for applications at high temperature. In particular, alumina scales developed on high-temperature alloys are one of the most protective films. It is well known that active elements such as yttrium (or others) notably increase the alumina scale adherence, but despite extensive work on this subject the mechanisms by which such elements act are not yet elucidated [1]. Many authors suggest that yttrium can act on the transport properties of alumina scales, which seems confirmed by extensive work on massive aluminas [2–13]. Nevertheless, in the case of alumina scales various and sometimes opposite mechanisms are suggested in order to explain the effect of yttrium on the transport properties. For instance, according to the preponderant diffusion (cationic or anionic) which ensures alumina scale growth, it is proposed that yttrium either decreases aluminium diffusion [14] or oxygen diffusion [15, 16]. However, it must be remarked that there is not a great scatter in the parabolic oxidation constant values found by various authors.

The problem with alumina is that it is one of the most stoichiometric oxides and, consequently, its transport properties are dominated by the impurities. In addition there is a lack of data about self-diffusion in alumina, particularly aluminium diffusion and also grain-boundary diffusion of both aluminium and oxygen [8, 17–24]. Due to these two disadvantages, it is not possible at this date to compare cationic and anionic diffusion coefficients.

Thus, it appeared necessary to perform new aluminium and oxygen self-diffusion experiments in alumina, on the same materials treated in the same conditions and with the same procedure, in order to be able to perform a correct comparison of oxygen

0022–2461

and aluminium diffusivities in the bulk and in the grain boundaries [8, 25, 26].

In order to apply the results to the interpretation of the effect of yttrium on the growth rate of alumina scales, it is necessary to determine the diffusion coefficients in undoped and yttrium-doped aluminas. This has been conducted for oxygen diffusion, using the previous results obtained by Prot [8] on undoped single crystals and polycrystalline alumina samples, and measuring the oxygen diffusivity on materials differing only in the presence of a doping element [26, 27].

2. Experimental procedure

2.1. Materials

α-Al_2O_3 single crystals were elaborated by the Verneuil technique by Baikowski Chimie Society for both the undoped alumina samples used by Prot [8] and the doped samples. In this case the single crystals were made from a 300 p.p.m. (weight percentage) Y_2O_3-doped alumina powder of the same purity as the powder used for the undoped samples. The powder doping procedure is described elsewhere [26]. Chemical analyses indicated that the undoped and doped aluminas were contaminated by silicon. The samples were prepared so that the surface for diffusion experiments was parallel to the (0 0 0 1) plane.

Dense polycrystals of good quality were obtained by hot pressing (performed by P. Carry, Ecole Polytechnique de Lausanne) [27], using a 500 p.p.m. Y_2O_3-doped alumina powder also provided by Baikowski Chimie Society. These polycrystals had a volumic mass equal to 99.6% of the theoretical volumic mass of alumina. Again a contamination with Si was detected.

All samples were accurately diamond-polished and then annealed in 0.21 atm $^{16}O_2$ or in air for oxygen and aluminium diffusion experiments, respectively, at a temperature corresponding to the diffusion test conditions and during a sufficiently long time to ensure equilibrium as much as possible. As will be shown later, in doped samples yttrium segregation can occur during this pre-annealing.

$^{18}O_2$ was obtained through CEA (France) and was introduced by isotopic exchange [26]. A low-activity solution of ^{26}Al was provided by the Los Alamos National Laboratory (LANL) and deposited as a drop on the sample surface [25]. Afterwards, diffusion annealing was conducted in air.

The diffusion experiments were conducted between 1540 and 1697° C for aluminium diffusion and 1110–1630° C for oxygen diffusion. All our conditions were similar to those used by Prot [8].

2.2. Depth profiling

For all determinations of the oxygen diffusion coefficients, depth profiling was performed by secondary ion mass spectrometry (SIMS) (CNRS, Bellevue). The samples were previously covered by a thin layer of Au ($\sim$ 20 nm) in order to eliminate charges, and the analysis conditions were the following: 10 keV Cs^+ ion source, scanned area 250 μm $\times$ 250 μm, analysed zone 62 μm in diameter [26]. After having verified that a constant sputtering rate was obtained (linear relation between crater depth and analysis time), the penetration depths were deduced by measuring the final depth of the crater by means of a profilometer.

In case of aluminium diffusion, the curves for activity versus depth were established by successive thin mechanical abrasions ($\sim$ 0.05 μm) and by counting each time the residual activity (A_r) of the sample using the γ disintegration ray of ^{26}Al (0.511 MeV) and a germanium detector (Marseille laboratory) [25].

2.3. Determination of diffusion coefficients

The diffusion coefficients were computed using the following equations.

(i) For oxygen lattice diffusion coefficients

$$\frac{C(y,t) - C_s}{C_\infty - C_s} = \mathrm{erf}\left(\frac{y}{2(D_L t)^{1/2}}\right) \tag{1}$$

with y the penetration depth, C_s the constant superficial concentration in ^{18}O, C_∞ the natural isotopic concentration and D_L the lattice diffusion coefficient.

(ii) For aluminium lattice diffusion coefficients

$$A_r = A_{r(0)}\,\mathrm{erfc}\left(\frac{y}{(4D_L t)^{1/2}}\right) \tag{2}$$

with $A_{r(0)}$ the total tracer activity per surface unit at $y = 0$.

(iii) For diffusion along dislocations if isolated

$$\frac{\partial \ln \bar{C}}{\partial y} = -\frac{A(\alpha)}{\left[\left(\frac{D_d}{D_L} - 1\right)u^2\right]^{1/2}} \tag{3}$$

with A a coefficient whose value is given by the curve of A versus α [28]; α is the reduced value of the dislocation radius, $u/(D_L t)^{1/2}$, u being the radius of the dislocation, and D_d is the dislocation diffusion coefficient.

(iv) For diffusion either along aligned dislocations (sub-boundaries) or grain boundaries (Whipple–Le Claire equation for B-type diffusion)

$$\delta_{gb} D_{gb} = 1.322\left(\frac{D_L}{t}\right)^{1/2}\left(-\frac{\partial \ln \bar{C}}{\partial y^{6/5}}\right)^{-5/3} \tag{4}$$

with δ_{gb} (or δ_{sb}) the grain boundary (or sub-boundary) thickness and D_{gb} (or D_{sb}) the grain boundary (or sub-boundary) diffusion coefficient.

In all cases, for oxygen diffusion the ^{18}O concentration was calculated from the results of SIMS analysis using

$$[^{18}O] = I(18)/[I(16) + I(18)]$$

where $I(M)$ is the intensity in counts per second of the mass M.

3. Results

3.1. Oxygen and aluminium lattice diffusion coefficients in undoped α-alumina

The lattice diffusion coefficients of oxygen [8] and aluminium [25] in single crystals of α-alumina are

reported in Fig. 1 and compared with literature data for oxygen and aluminium self-diffusion [17–24] and cationic heterodiffusion [29, 30]. It appears that aluminium and oxygen diffusion coefficients determined in the same material with the same experimental conditions [8, 25] are of the same order of magnitude. Aluminium diffusion is somewhat greater than oxygen diffusion but the difference is very small.

Aluminium diffusion coefficients determined in our single crystals [25] are three to four orders of magnitude smaller than those determined byPaladino and Kingery [17] in polycrystalline samples. The coefficients determined in our single crystals are also smaller than the cationic heterodiffusion coefficients determined by Lesage [29] and Badrour [30] on mono- and polycrystalline alumina samples.

The oxygen diffusion coefficients in single crystals are smaller than most of the literature data on oxygen diffusion, except for the diffusion coefficients of Oishi *et al.* [20] and Reed and Wuench [21]. They are exactly in agreement with the oxygen diffusion determined by Lagerlof *et al.* [23] and Cadoz [24].

Concerning the coefficients determined in our single crystals of undoped alumina, the values of the diffusion coefficients are collected in Table I. In the case of oxygen diffusion [8], the diffusion law deduced from the Arrhenius graph (Fig. 2) is

$$D_L^O(\mathrm{cm^2\,s^{-1}}) = 206(\mathrm{cm^2\,s^{-1}}) \times \exp[-636 \pm 30(\mathrm{kJ\,mol^{-1}})/RT]$$

Such a value of the activation energy for oxygen lattice diffusion in alumina is of the same order of magnitude as most of the results shown in Fig. 1 for oxygen diffusion.

In the case of aluminium diffusion, if one attempts to determine an activation energy from the few points one finds 510 kJ mol^{-1}, whereas Paladino and Kingery [17] found an activation energy equal to 460 kJ mol^{-1}.

It should be noted that the value at 1697° C for aluminium diffusion is doubtful: it corresponds to the determination of a lattice diffusion coefficient on a curve which looks like a curve tail. It means that this point corresponds rather to an apparent diffusion coefficient than to a lattice diffusion coefficient, with $D_{app} = \lambda D_{sb} + (1 - \lambda)D_L$, λ being the fraction of atoms which diffuse in sub-boundaries. This point has not been taken into acccount in Fig. 2 for the calculation of an order of magnitude of the activation energy.

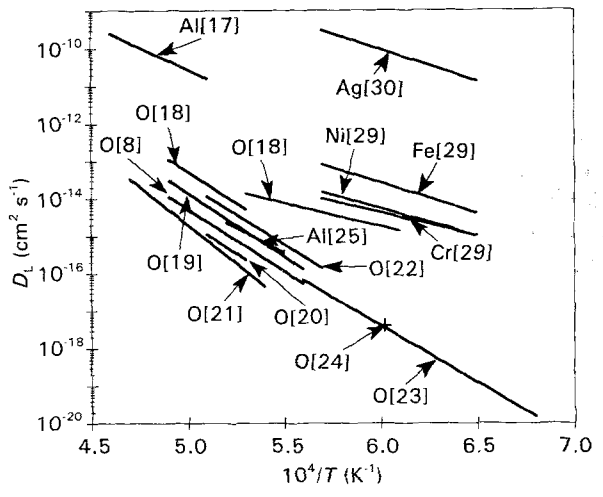

Figure 1. Temperature dependence of aluminium and oxygen lattice diffusion in undoped α-alumina. Our results for single crystals and literature data.

TABLE I Lattice diffusion coefficients of oxygen and aluminium determined in single crystals of undoped α-alumina.

T(° C)	$10^4/T$ (K^{-1})	t(h)	D_L^O (cm^2 s^{-1}) [8]	D_L^{Al}(cm^2 s^{-1}) [25]
1500	5.64	10	4.6×10^{-17}	
1520	5.58	5.5	5.1×10^{-17}	
1540	5.515	253.25		4×10^{-16}
1550	5.49	3	1.0×10^{-16}	
1570	5.43	3	2.1×10^{-16}	
1570	5.43	6	3.7×10^{-16}	
1577	5.40	2	2.0×10^{-16}	
1577	5.40	6	1.9×10^{-16}	
1600	5.34	24	3.5×10^{-16}	
1610	5.31	100		8×10^{-16}
1630	5.25	5	9.4×10^{-16}	
1630	5.25	24	6.1×10^{-16}	
1630	5.25	84	5.4×10^{-16}	
1650	5.20	214.5		3×10^{-15}
1660	5.17	24	1.2×10^{-15}	
1685	5.11	80	3.1×10^{-15}	
1697	5.076	49.75		(9.8×10^{-14})
1720	5.02	72	4.2×10^{-15}	

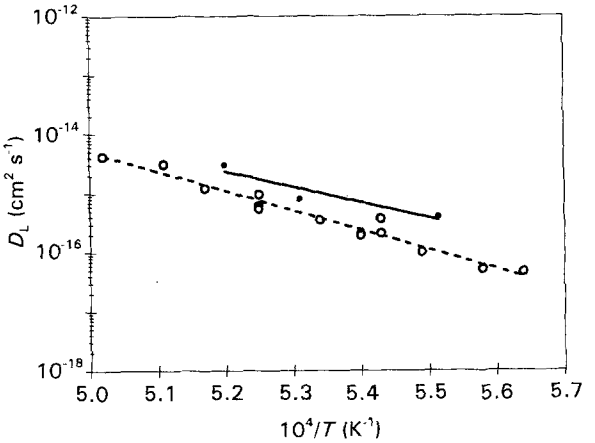

Figure 2. Arrhenius plot of the lattice self-diffusion in single crystals of undoped α-alumina: (○,---) O, AE = 636 kJ mol^{-1} [8]; (●, ——) Al, AE ~ 510 kJ mol^{-1} [25, 26].

3.2. Oxygen and aluminium sub-boundary diffusion coefficients in undoped α-alumina

It was verified by transmission electron microscopy (TEM) that the penetration curve tails were due to diffusion along sub-boundaries (i.e. aligned dislocations) in the alumina single crystal. It was verified [8], by the evolution of the curves $\ln(C - C_\infty) = f(y^{6/5})$ as a function of the diffusion time, that the slope of the curve tail depends on the diffusion time which excludes isolated dislocations. Thus Equation 4 was used.

TABLE II. Sub-boundary diffusion coefficients of oxygen and aluminium determined in single crystals of undoped α-alumina

T (°C)	$10^4/T$ (K^{-1})	t (h)	D_{sb}^{O} ($cm^2 s^{-1}$) [8]	D_{sb}^{Al} ($cm^2 s^{-1}$) [25]	$\Delta = D_{sb}/D_L$
1500	5.64	10	8.3×10^{-13}		2.1×10^4
1520	5.58	5.5	2.9×10^{-12}		4.6×10^4
1540	5.515	253.25		$2.2\text{–}3.4 \times 10^{-11}$	$5.5\text{–}8.5 \times 10^4$
1550	5.49	3	7.3×10^{-12}		5.8×10^4
1570	5.43	3	3.2×10^{-11}		1.6×10^5
1570	5.43	6	2×10^{-11}		1×10^5
1577	5.40	2	1.1×10^{-11}		4.7×10^4
1577	5.40	6	8.9×10^{-12}		3.8×10^4
1600	5.34	24	2.2×10^{-11}		5.7×10^4
1600	5.34	94	1.1×10^{-10}		2.8×10^5
1610	5.31	100		$6\text{–}9 \times 10^{-10}$	$7.5\text{–}10.0 \times 10^5$
1630	5.25	5	3.8×10^{-11}		5.1×10^4
1630	5.25	24	4.5×10^{-11}		6.1×10^4
1630	5.25	84	1.9×10^{-10}		2.6×10^5
1650	5.20	80	1.6×10^{-10}		1.4×10^5
1650	5.20	214.5		3×10^{-9}	1×10^6
1660	5.17	24	2.0×10^{-10}		1.5×10^5
1675	5.13	118	1.0×10^{-10}		5.4×10^4
1685	5.11	80	3.5×10^{-10}		1.5×10^5
1697	5.076	49.75		$1\text{–}4.4 \times 10^{-9}$	$1\text{–}4.5 \times 10^4$
1707	5.05	72	7.3×10^{-10}		2.1×10^5
1720	5.02	72	9.2×10^{-10}		2.0×10^5
1751	4.94	67	4.8×10^{-9}		5.9×10^5

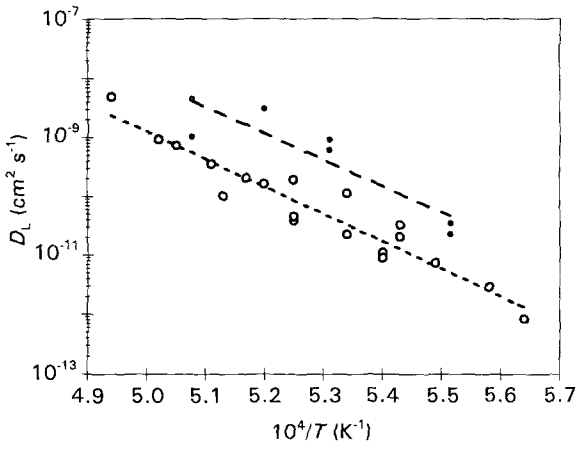

Figure 3. Arrhenius plot of the sub-boundary self-diffusion in single crystals of undoped α-alumina: (○,- - -) O, AE = 896 kJ mol^{-1} [8]; (●, ——) Al, AE = 850 kJ mol^{-1} [25, 26].

The values of the sub-boundary oxygen and aluminium diffusion coefficients in undoped α-alumina single crystals are collected in Table II. Fig. 3 shows the Arrhenius plot of these coefficients.

It appears that aluminium sub-boundary diffusion is faster than oxygen sub-boundary diffusion. The difference is more marked than in the case of lattice diffusion (see Fig. 2). The activation energy for the oxygen sub-boundary diffusion is equal to 896 kJ mol^{-1} [8] with a diffusion law given by

$$D_{sb}^{O}(cm^2 s^{-1}) = 3.1 \times 10^{14}(cm^2 s^{-1}) \times \exp[-896(kJ\,mol^{-1})/RT]$$

the thickness of the sub-boundary δ_{sb} being arbitrarily taken as 3×10^{-8} cm.

In the same manner as for aluminium lattice diffusion, if one attempts to determine an activation energy from the few points concerning aluminium sub-boundary diffusion, one finds 850 kJ mol^{-1}. In both cases (aluminium and oxygen diffusion), it is surprising to observe that the activation energy of sub-boundary diffusion is greater than the activation energy of lattice diffusion for the same element.

3.3. Oxygen lattice and sub-boundary diffusion coefficients in yttrium-doped α-Alumina

These results will be compared with the oxygen lattice and sub-boundary diffusion coefficients obtained by Prot [8] on single crystals of undoped α-alumina, whereas our samples are doped with 300 wt p.p.m. Y_2O_3 [26, 27]. In the case of Y-doped alumina, oxygen diffusion in sub-boundaries occurs for temperature higher than 1400° C. It was also verified by TEM observations, and by the evolution of the diffusion profiles as a function of diffusion time, that the curve tails were due to aligned dislocations (sub-boundaries) [26, 27].

Values of the diffusion coefficients found by Prot in undoped alumina are already given in Tables I and II. The values of oxygen diffusion coefficients in Y-doped alumina single crystals are collected in Table III for lattice and sub-boundary diffusion.

All these results are plotted in an Arrhenius graph in Fig. 4. The diffusion laws for oxygen diffusion in undoped alumina were already given above. In the case of Y-doped alumina

$$D_L^{O}(cm^2 s^{-1}) = 67(cm^2 s^{-1}) \times \exp[-590 \pm 30(kJ\,mol^{-1})/RT]$$

$$D_{sb}^{O}(cm^2 s^{-1}) = 10^{17}(cm^2 s^{-1}) \times \exp[-980(kJ\,mol^{-1})/RT]$$

TABLE III Lattice and sub-boundary diffusion coefficients of oxygen determined in single crystals of Y-doped alumina (300 wt p.p.m. Y_2O_3)

T (°C)	$10^4/T$ (K^{-1})	t (h)	D_L^o ($cm^2 s^{-1}$) [26, 27]	D_{sb}^o ($cm^2 s^{-1}$) [26, 27]	$\Delta = D_{sb}/D_L$	β
1110	7.23	6	7.6×10^{-18}–3.2×10^{17}			
1110	7.23	6	2.7×10^{-18}–2.2×10^{-17}			
1250	6.56	54.3	8.0×10^{-19}			
1345	6.18	6	1.3×10^{-17}			
1370	6.08	5.5	1.6×10^{-17}			
1396	5.99	5	2.3×10^{-17}			
1415	5.92	80	2.0×10^{-17}	1.8×10^{-14}	9.2×10^{2}	6
1460	5.77	54.3	3.0×10^{-17}	9.2×10^{-13}	3.0×10^{4}	200
1497	5.65	44.5	1.5×10^{-16}	8.9×10^{-12}	5.9×10^{4}	190
1505	5.62	2	1.4×10^{-16}	1.0×10^{-11}	7.5×10^{4}	1174
1550	5.48	24	1.1×10^{-15}	8.0×10^{-11}	7.3×10^{4}	118
1550	5.48	5.1	4.5×10^{-15}	8.6×10^{-10}	1.9×10^{5}	332
1600	5.34	8	1.9×10^{-15}	1.0×10^{-10}	5.5×10^{4}	117
1600	5.34	8	8.4×10^{-16}	7.3×10^{-11}	8.7×10^{4}	278
1614	5.30	3.1	3.0×10^{-15}	6.4×10^{-11}	2.1×10^{4}	54
1630	5.25	5.5	1.0×10^{-14}	8.0×10^{-10}	8.0×10^{4}	90
1630	5.25	5.25	1.7×10^{-14}	8.6×10^{-10}	5.0×10^{4}	44

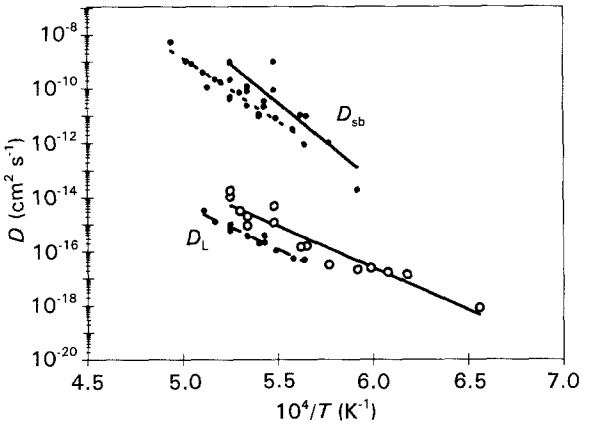

Figure 4. Arrhenius plot of the lattice and sub-boundary diffusion of oxygen in single crystals of undoped and Y-doped α-alumina (300 wt p.p.m. Y_2O_3). Undoped [8]: (○,--) D_L, (●,---) D_{sb}. Y-doped [26, 27]: (○,——) D_L, (●,——) D_{sb}.

It again appears for Y-doped alumina that the activation energy of sub-boundary diffusion is greater than the activation energy of lattice diffusion. In undoped and Y-doped alumina single crystals, the order of magnitude of both the activation energy of lattice diffusion and the activation energy of sub-boundary diffusion can be considered as of the same order of magnitude due to the uncertainty. In both the lattice and the sub-boundaries, yttrium doping slightly increases the diffusion coefficients.

3.4. Oxygen grain-boundary diffusion coefficients in yttrium-doped α-alumina

Again, these results will be compared with the oxygen grain-boundary diffusion coefficients obtained by Prot [8] on polycrystalline undoped alumina samples, while ours are doped with 500 wt p.p.m. Y_2O_3 [26, 27].

TABLE IV Grain boundary diffusion coefficients of oxygen determined in undoped and Y-doped polycrystalline alumina samples (500 wt p.p.m. Y_2O_3)

T (°C)	$10^4/T$ (K^{-1})	t (h)	D_{gb}^o ($cm^2 s^{-1}$)		$\Delta = D_{gb}/D_L$	β
			Undoped [8]	Y-doped [26, 27]		
1460	5.77	1.9		4×10^{-14}	4.9×10^{2}	30
1460	5.77	1.9		6.6×10^{-14}	2.5×10^{2}	15
1499	5.64	2	8.9×10^{-12}		2.3×10^{5}	2×10^{4}
1505	5.62	2		5×10^{-13}	2.5×10^{3}	85
1540	5.51	1	9.7×10^{-11}		9.6×10^{5}	8×10^{4}
1550	5.48	2.1		2.1×10^{-13}	3.7×10^{2}	8
1580	5.40	2	1.7×10^{-10}		6.8×10^{5}	3×10^{4}
1580	5.40	8.1		7.2×10^{-13}	5.5×10^{2}	4
1614	5.30	3.1		1.6×10^{-11}	1.7×10^{3}	15
1629	5.26	6.5	3.1×10^{-10}		4.3×10^{5}	5×10^{3}
1660	5.17	0.5	1.8×10^{-9}		1.3×10^{6}	4×10^{4}
1689	5.10	3	6.0×10^{-9}		2.4×10^{6}	2×10^{4}
1718	5.02	6.5	1.5×10^{-8}		3.4×10^{6}	2×10^{4}

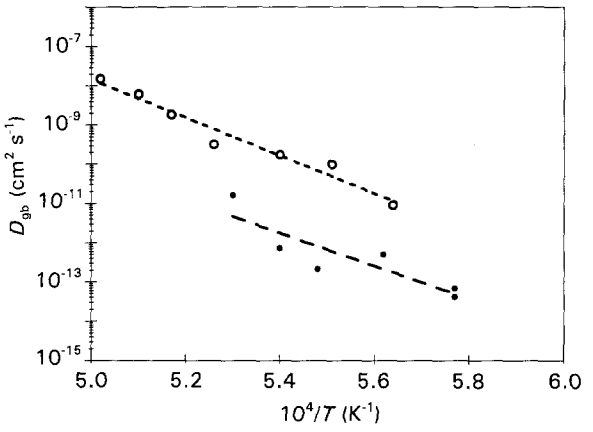

Figure 5. Arrhenius plot of the grain-boundary diffusion of oxygen in undoped and Y-doped α-alumina (500 wt p.p.m. Y_2O_3): (○,---) undoped [8], AE = 921 kJ mol^{-1}; (○,---) Y-doped, AE = 800 kJ mol^{-1} [26, 27].

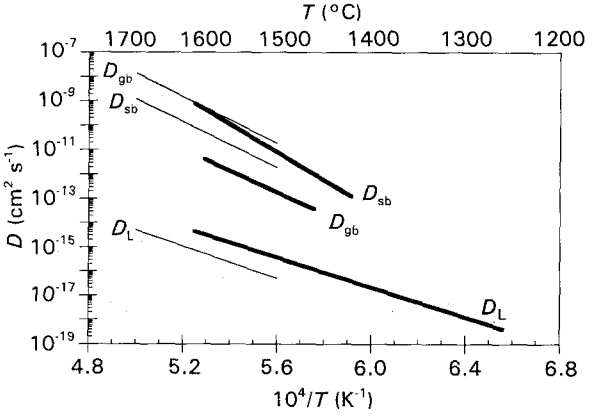

Figure 6. Comparisons of lattice, sub-boundary and grain-boundary diffusion of oxygen in (——) undoped [8] and (—) Y-doped [26, 27] aluminas.

The values of the grain-boundary diffusion coefficients obtained in polycrystalline undoped [8] and Y-doped α-alumina are collected in Table IV. All these results are plotted in an Arrhenius graph in Fig. 5. The diffusion laws are the following: in the case of undoped alumina

$$D^{O}_{gb}(\mathrm{cm^2\,s^{-1}}) = 1.6 \times 10^{16}(\mathrm{cm^2\,s^{-1}}) \times \exp[-921(\mathrm{kJ\,mol^{-1}})/RT]$$

while in the case of Y-doped alumina

$$D^{O}_{gb}(\mathrm{cm^2\,s^{-1}}) = 7 \times 10^{10}(\mathrm{cm^2\,s^{-1}}) \times \exp[-800 \pm 20(\mathrm{kJ\,mol^{-1}})/RT]$$

where δ_{gb} is taken as 1 nm. It appears that the oxygen grain-boundary diffusion coefficients are smaller in Y-doped alumina than in undoped alumina by about three orders of magnitude.

The activation energy can be considered of the same order of magnitude for undoped and doped aluminas. The activation energy of grain-boundary diffusion, like the activation energy of sub-boundary diffusion, is greater than the activation energy of lattice diffusion.

If all the results concerning oxygen diffusion obtained by Prot [8] and ourselves [26, 27] are plotted on the same graph (Fig. 6), it appears that in undoped alumina the sequence is

$$D_L < D_{sb} < D_{gb}$$

as generally observed, while in Y-doped alumina the sequence is

$$D_L < D_{gb} < D_{sb}$$

4. Discussion

As the results obtained by Prot and co-workers [8, 31] and Le Gall *et al.* [25–27] have already been discussed in detail, only the main interpretations will be recalled here. Indeed, the objective of this paper is to use the comparative results obtained by these authors to get information on the growth mechanism of alumina scales formed by high-temperature oxidation, and on the yttrium effect on high-temperature corrosion resistance.

4.1. Self-diffusion mechanisms in alumina

4.1.1. Lattice self-diffusion

The theoretically undoped alumina single crystals used in the work of Prot *et al.* and Le Gall *et al.* [8, 25–27, 31] are unfortunately doped with silicon (50 wt p.p.m. in the original powder). This is a non-negligible amount for alumina, which is a very stoichiometric oxide; Dils [32] suggests that at 1727° C the scatter from stoichiometry is equal to $\sim 10^{-8}$. Considering this and the low values of the activation energy of lattice diffusion, it is suggested that extrinsic diffusion occurs. Then the results obtained for oxygen and aluminium lattice diffusion can be justified on the basis of the preponderant impurity, i.e. Si.

In the case of oxygen diffusion, Prot [8] showed that the lattice extrinsic diffusion mechanism could only be interpreted assuming that the impurity Si in alumina was compensated by oxygen interstitials, O_i''. This interpretation was in agreement with the calculated possible defect concentrations, with the activation energy (636 kJ mol^{-1}) equal to the migration enthalpy of the oxygen interstitial and with the entropy term in the preexponential factor. With Prot's considerations, it is found that $[O_i''] = 25$ p.p.m. and then it can be deduced that $[V'''_{Al}] \simeq 4$ p.p.m. In such a case, considering that aluminium self-diffusion also occurs by an extrinsic diffusion mechanism, the respective diffusion rates of Al and O would mainly depend on the differences between the activation enthalpies for the defect considered. Our results are perhaps too limited to propose an activation energy, but calculations made by Dienes *et al.* [33] give for the migration enthalpy of V'''_{Al} a value equal to 366 kJ mol^{-1}. The difference between the two migration enthalpies can explain the greater diffusivity of aluminium. Anyway, it must be remembered that both oxygen and aluminium diffusions occur by an extrinsic mechanism and that the aluminium diffusivity is somewhat greater, with a slightly smaller activation energy.

4.1.2. Sub-boundary diffusion

In "undoped" alumina, the sub-boundary diffusion coefficients of aluminium are greater than those concerning oxygen diffusion. This was explained by Le Gall *et al.* [25, 26] by the size differences between aluminium and oxygen ions ($R_{Al^{3+}} = 0.053$ nm and $R_{O^{2-}} = 0.138$ nm) and by the fact that oxygen ions have a greater affinity for cations segregated along the sub-boundaries than aluminium ions. In both cases, the activation energy of sub-boundary diffusion would be equal to the sum of the defect migration enthalpy and of an interaction enthalpy term (interaction between the diffusing species and the segregated impurities). Both the migration term and the interaction enthalpy term would be greater in the case of oxygen diffusion.

4.1.3. Grain-boundary diffusion

In "undoped" alumina only oxygen grain-boundary diffusion data are available. Comparisons between anionic and cationic diffusion cannot be performed. It must be remembered that the activation energy of oxygen grain-boundary diffusion is greater than the activation energy for lattice diffusion. It is suggested that this is again due to an interaction term between the diffusing species and the impurities segregated or precipitated along grain boundaries. It could be expected that the same phenomenon would occur for aluminium diffusion, probably less importantly, and always on account of the difference in the sizes of the two ions and in their respective affinities for the segregated impurities.

4.1.4. Effect of yttrium on oxygen diffusivity

As shown by Fig. 6, the yttrium doping of alumina induces a slight increase of oxygen lattice diffusion and of sub-boundary diffusion but a decrease of the oxygen grain-boundary diffusion.

In the case of lattice diffusion, the differences are explained by considering that the extrinsic lattice diffusion mechanism is now controlled by silicon and yttrium impurities which both act as a "donor", i.e. they induce an increase of oxygen interstitial defects [26, 27]. Considering, on the basis of the work of Loudjani *et al.* [34, 35], that only 10 p.p.m. yttrium atoms are in solid solution in alumina single crystals, the oxygen interstitial concentration has been evaluated as equal to 40 p.p.m. (always taking into account the 50 p.p.m. Si). This increase in the oxygen interstitial concentration compared to "undoped" alumina ($\sim$ 25 p.p.m.) explains the increase of the oxygen lattice diffusion coefficients. This is in agreement with the fact that the activation energy is of the same order of magnitude in both "undoped" and Y-doped materials.

In the case of sub-boundary diffusion, it is suggested that at temperatures lower than 1400° C yttrium is precipitated on sub-boundaries and notably decreases the oxygen sub-boundary diffusion (no curve tails were observed in these cases). At temperatures higher than 1400° C, yttrium precipitate dissolution occurs which induces a greater density of dislocations free for diffusion in the sub-boundaries than in undoped alumina. The slight increase of oxygen diffusion in doped alumina is due to the greater dislocation density resulting from the yttrium incorporation during elaboration of the samples on account of the important size of Y^{3+} ions. It results in an increase of the sub-boundary energy and diffusivity.

In the case of grain-boundary diffusion, yttrium decreases the oxygen diffusivity on account of the effect of either yttrium precipitates or yttrium segregation (according to the temperature [34, 35]) along the alumina grain boundaries [26, 27].

It is always observed that the activation energy of sub-boundary and grain boundary diffusion is greater than the activation energy (AE) of lattice diffusion, always on account of the fact that $(AE)_L = \Delta H_m$ when $(AE)_{sb \text{ or } gb} \simeq \Delta H_m + \Delta H_{int}$, as discussed above.

4.2. Relation between diffusion and growth of alumina scales formed by oxidation of alloys at high temperature

Though all the results concerning self-diffusion in a given alumina material are not available (there is a lack of data for grain-boundary diffusion of aluminium), it is interesting now to calculate the parabolic oxidation constants k_c from the various possible diffusion mechanisms and to compare them with the literature data on k_c values given by oxidation experiments.

Using Wagner's theory [36], and considering that the diffusion coefficients do not vary with oxygen pressure, which is suggested by Prot [8], k_c can be written

$$k_c = \int_{pO_2(i)}^{pO_2(e)} (1.5\, D_{eff}^{Al} + D_{eff}^{O})\, d(\ln pO_2)$$

with $pO_2(i)$ and $pO_2(e)$ the oxygen pressure at the inner and outer interfaces of the alumina scale, respectively, and D_{eff}^{Z} the effective diffusion coefficient of the Z element given by

$$D_{eff}^{Z} = (1 - f - \lambda) D_L + f D_{gb} + \lambda D_{sb}$$

with f the volume fraction of grain boundaries: $f = 3\,\delta/\Phi$ where δ is the grain boundary width (taken as 1 nm) and Φ the diameter of the grains (taken equal to 1 μm which is an average value for alumina grains in oxide scales), giving $f = 3 \times 10^{-3}$. λ is the volumic fraction of sub-boundaries given by $\lambda = \pi u^2 \rho_d$, with u the dislocation radius ($u \simeq 1$ nm) and ρ_d the dislocation density whose maximum value must be about 10^{10} cm cm^{-3} [26]; this gives $\lambda = 3 \times 10^{-4}$. Thus

$$(1 - f - \lambda) \simeq 1.$$

The calculations will be conducted at two temperatures, 1100 and 1300° C, by extrapolating the self-diffusion results obtained by Prot and Le Gall in "undoped" alumina and in Y-doped alumina [8, 25–27, 31]. This will possibly yield evidence of an inversion in the main diffusion phenomenon, as suggested by some authors in the case of yttrium-doped alumina scale growth [37, 38]. For these temperatures, the order of magnitude of experimental k_c values

TABLE V. Diffusion contributions at 1100 and 1300° C for oxygen and aluminium in "undoped" and Y-doped aluminas, calculated by extrapolation of the previous data

Parameter ($cm^2 s^{-1}$)	1100° C ($10^4/T$ = 7.28 K^{-1})		1300° C ($10^4/T$ = 6.35 K^{-1})	
	Undoped	Y-doped	Undoped	Y-doped
D_L^O	1×10^{-22}	2×10^{-21}	2×10^{-19}	2×10^{-18}
D_{sb}^O	2×10^{-20}	5×10^{-21}	5×10^{-16}	3×10^{-16}
λD_{sb}^O	6×10^{-24}	1×10^{-24}	2×10^{-19}	8×10^{-20}
D_{gb}^O	1×10^{-19}	2×10^{-20}	4×10^{-15}	2×10^{-16}
fD_{gb}^O	3×10^{-22}	7×10^{-23}	1×10^{-17}	6×10^{-19}
D_{eff}^O	4×10^{-22}	2×10^{-21}	1.2×10^{-17}	2.69×10^{-18}
D_L^{Al}	6×10^{-21}		2×10^{-18}	
D_{sb}^{Al}	6×10^{-19}		7×10^{-15}	
λD_{sb}^{Al}	2×10^{-22}		2×10^{-18}	
D_{gb}^{Al}	*2.5×10^{-18}*		*5.6×10^{-14}*	
fD_{gb}^{Al}	*7×10^{-21}*		*2×10^{-16}*	
D_{eff}^{Al}	1.34×10^{-20}		1.68×10^{-16}	

(found in oxidation experiments) is

$$k_c \simeq 5\times10^{-13}\text{–}10^{-12}\,cm^2\,s^{-1} \quad \text{at } 1100°\,C$$
$$\simeq 10^{-11}\,cm^2\,s^{-1} \quad \text{at } 1300°\,C$$

In these temperature conditions

$$\ln\left(\frac{pO_2(e)}{pO_2(i)}\right) = 75.9 \quad \text{at } 1100°\,C$$
$$= 59.8 \quad \text{at } 1300°\,C$$

with $pO_2(i) = 10^{-32}$ atm at 1100° C and 10^{-25} atm at 1300° C, if thermodynamic equilibrium is reached and in standard conditions.

The different oxygen diffusion laws in "undoped" alumina (this work and Prot's work) are the following, $D°$ being expressed in $cm^2\,s^{-1}$ and the activation energy in kJ mol^{-1}:

$$D_L^O = 206\exp(-636/RT)$$
$$D_{sb}^O = 3.1\times10^{14}\exp(-896/RT)$$
$$D_{gb}^O = 1.6\times10^{16}\exp(-921/RT)$$

In the case of aluminium diffusion in undoped alumina, the estimated laws are

$$D_L^{Al} = 0.16\exp(-510/RT)$$
$$D_{sb}^{Al} = 1.3\times10^{14}\exp(-850/RT)$$

The diffusion coefficients deduced from these laws at 1100 and 1300° C are collected in Table V. Due to the lack of data on aluminium grain-boundary diffusion, it has been assumed that the ratio D_{gb}/D_{sb} was a constant for oxygen and aluminium diffusion. Then D_{gb}^{Al} has been calculated. The hypothetical values are given in italics in Table V.

4.2.1. Results at 1100° C

With all the considerations given and assuming that

$$\frac{D_{sb}^{Al}}{D_{sb}^O} \simeq \frac{D_{gb}^{Al}}{D_{gb}^O} \simeq 24$$

it is observed that aluminium grain-boundary diffusion would be the preponderant phenomenon with

$$fD_{gb}^{Al} = 7\times10^{-21}\,cm^2\,s^{-1} > \lambda D_{sb}^{Al}$$
$$D_{eff}^O \ll D_{eff}^{Al} = 1.3\times10^{-20}\,cm^2\,s^{-1}$$

Then

$$k_c = 1.5(D_L^{Al} + fD_{gb}^{Al})\ln\left(\frac{pO_2(e)}{pO_2(i)}\right)$$
$$= 1.5\times10^{-18}\,cm^2\,s^{-1}$$

which is $\ll 10^{-13}\,cm^2\,s^{-1}$ (the experimental k_c value).

4.2.2. Results at 1300° C

In this case, assuming

$$\frac{D_{sb}^{Al}}{D_{sb}^O} \approx \frac{D_{gb}^{Al}}{D_{gb}^O} \simeq 14$$

it appears that

$$fD_{gb}^{Al} = 1.7\times10^{-16}\,cm^2\,s^{-1} > \lambda D_{sb}^{Al}$$
$$= 2\times10^{-18}\,cm^2\,s^{-1}$$
$$fD_{gb}^{Al} > fD_{gb}^O \simeq 10^{-17}\,cm^2\,s^{-1}$$

Then

$$k_c = 1.5fD_{gb}^{Al}\ln\left(\frac{pO_2(e)}{pO_2(i)}\right) = 1.5\times10^{-14}\,cm^2\,s^{-1}$$

which is $\ll 10^{-11}\,cm^2\,s^{-1}$ (the experimental k_c value).

4.2.3. Summary

The results appear to show the following.

(i) Whatever the temperature, aluminium diffusion should predominate over oxygen diffusion, at least in the case of growth of alumina scales doped with donor elements (since our "undoped" alumina single crystals are doped with silicon). Clearly, the literature data indicate that alumina scale growth is often controlled by oxygen diffusion [14, 39, 40], even if cationic diffusion is observed in some cases (NiAl alloy, for instance [15, 41], but in this case Ni is incorporated in the scale [42] and should act as an acceptor).

(ii) In all cases, it is clear that lattice diffusion alone cannot explain the growth rate of alumina scales.

(iii) Even considering intergranular diffusion, the oxidation constants calculated from these coefficients are smaller than the experimental oxidation constants. This was already observed by Sabioni *et al.* [43] in the case of chromia scale, and it is an object of controversy in the case of NiO scales [44–46]. This suggests that grain boundaries and all diffusion short-circuits can chemically and physically differ according to the elaboration mode of the polycrystals (i.e. polycrystals grown from the melt or obtained by sintering or by oxidation). Differences in the mass transport rates could also be due to differences in the impurity nature and amount in scales and in massive oxides, and modifications of the purity of scales can occur as growth proceeds [47]. Another parameter which should be considered consists in the fact that, in the case of Al_2O_3 scale growth, other Al oxide phases

(γ- and θ-Al_2O_3, particularly) can form before α-Al_2O_3 nucleates and grows [48].

4.3. Effect of yttrium on the growth mechanism of alumina scales

Calculations similar to those made in the previous sections can be made for Y-doped alumina. In this case, only oxygen diffusion results are available. The diffusion laws are the following

$$D_L^O = 67 \exp(-590/RT)$$

$$D_{sb}^O = 1 \times 10^{17} \exp(-980/RT)$$

$$D_{gb}^O = 7 \times 10^{10} \exp(-800/RT)$$

The various diffusion contributions were then calculated at 1100 and 1300° C as previously (Table V).

4.3.1. Results at 1100° C

In this case, considering only oxygen diffusion, it is the lattice diffusion contribution which predominates. Then

$$k_c = D_L^O \ln\left(\frac{pO_2(e)}{pO_2(i)}\right) = 1.5 \times 10^{-19}\ cm^2\ s^{-1}$$

which is $\ll 10^{-13}\ cm^2\ s^{-1}$ (the experimental k_c value).

4.3.2. Results at 1300° C

At this temperature lattice, sub-boundary and grain-boundary diffusion will participate in the scale growth and

$$k_c = (D_L^O + \lambda D_{sb}^O + f D_{gb}^O) \ln\left(\frac{pO_2(e)}{pO_2(i)}\right)$$

$$\simeq 1.6 \times 10^{-16}\ cm^2\ s^{-1}$$

which is $\ll 10^{-11}\ cm^2\ s^{-1}$ (the experimental k_c value).

4.3.3. Summary

The values given above are smaller than those found in "undoped" alumina, but further interpretation is not possible as aluminium diffusion data are not available in this case. Nevertheless, as shown in Fig. 6, by the values in Table V and by the considerations in the next section, if alumina scales grow predominantly by short-circuit diffusion, as suggested by other authors [1, 39] it can be assumed that yttrium doping should decrease the growth rate of alumina scales on account of yttrium segregation and precipitation in the short-circuits. The increase of the growth rate observed by some authors for Y-doped alumina scales formed at high temperature when compared with the results obtained at lower temperature [37, 38] does not seem to be directly due to the presence of yttrium.

4.4. Comparison of self-diffusion coefficients in alumina and chromia

4.4.1. Lattice diffusion

The available lattice self-diffusion coefficients in massive undoped alumina [8, 25] and chromia [43] single crystals have been plotted in Fig. 7. In all cases, according to the authors' interpretations [8, 25, 43], diffusion is assumed to occur by an extrinsic mechanism. If the activation energies are compared, it means that the migration enthalpy ΔH_m of the defects responsible for the diffusion in alumina (oxygen interstitials and aluminium vacancies for oxygen and aluminium diffusion, respectively) is greater than the migration enthalpy of the defects responsible for the diffusion in chromia (chromium vacancies for chromium diffusion).

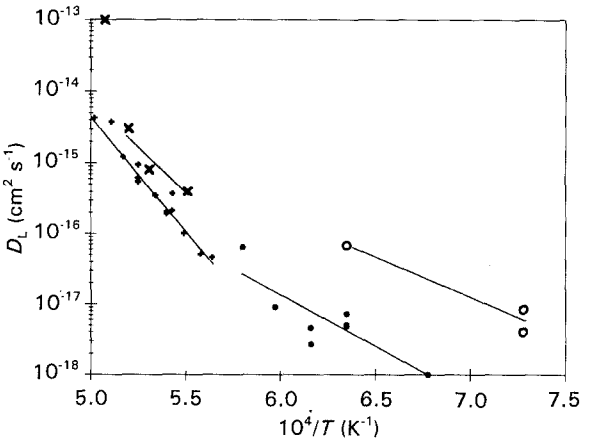

Figure 7. Arrhenius graph of lattice self-diffusion in Cr_2O_3 and Al_2O_3 undoped single crystals. (○) $Cr \rightarrow Cr_2O_3$ [43], AE = 280 kJ mol^{-1}; (○) $O \rightarrow Cr_2O_3$ [43], AE = 230 kJ mol^{-1}; (×) $Al \rightarrow Al_2O_3$ [25], AE = 510 kJ mol^{-1}; (×) $O \rightarrow Al_2O_3$ [8], AE = 636 kJ mol^{-1}.

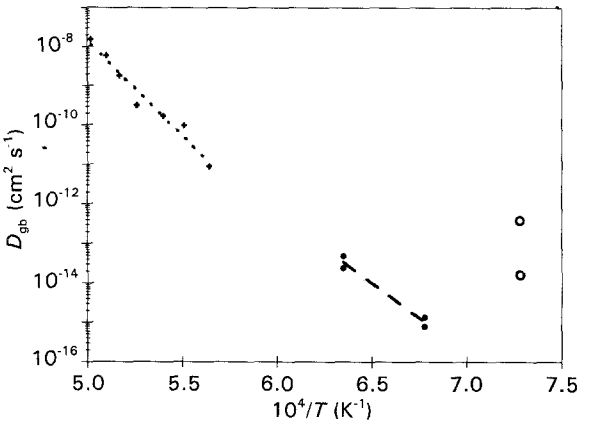

Figure 8. Arrhenius graph of grain-boundary self-diffusion in Cr_2O_3 and Al_2O_3 undoped polycrystals. (○, ---) $Cr \rightarrow Cr_2O_3$ [43]; (○) $O \rightarrow Cr_2O_3$ [43]; (+, ···) $O \rightarrow Al_2O_3$ [8], AE = 921 kJ mol^{-1}.

In the case of alumina, the diffusion coefficients of oxygen and aluminium are of the same order of magnitude, while in chromia the oxygen diffusion coefficient is greater than D_{Cr}. Whereas the growth rate of chromia oxide scales is about two orders of magnitude smaller than the growth rate of alumina scales [49], such a difference does not appear so clearly between the diffusion coefficients in massive oxides.

4.4.2. Grain-boundary diffusion

It appears from Fig. 8 that again there is not a great difference between the grain-boundary diffusion

coefficients of oxygen in massive alumina and chromium in massive chromia, elements which are assumed in most cases to be responsible for the scale growth. In both cases, it is observed that the activation energy of the grain-boundary diffusion is greater than the activation energy of the lattice diffusion, as already mentioned.

5. Conclusions

Lattice and grain-boundary diffusion coefficients of aluminium and oxygen in Al_2O_3 single crystals or polycrystalline samples were determined using ^{18}O tracer and depth profiling by SIMS or ^{26}Al and γ counting. For the first time, the aluminium and oxygen diffusion coefficients were determined in the bulk and along sub-boundaries, on the same materials (single crystals) treated in the same conditions. Oxygen grain-boundary diffusion was also determined on polycrystals. The conclusions were as follows.

1. Aluminium lattice diffusion coefficients are lower than values previously given in the literature. It can be suggested that the previous results obtained from polycrystals were relative to apparent diffusion coefficients, taking into account a part of grain boundary or sub-boundary diffusion. Oxygen lattice diffusion coefficients are in agreement with some of the values previously given in the literature.

2. In both cases, lattice diffusion occurs by an extrinsic mechanism controlled by silicon impurity. The activation enthalpy of lattice diffusion corresponds to the migration enthalpy of oxygen interstitial in case of oxygen diffusion, and to aluminium vacancy in case of aluminium diffusion.

3. Sub-boundary (Al and O) diffusion and grain-boundary oxygen diffusion are characterized by an activation energy greater than the activation energy of lattice diffusion on account of segregation phenomena. They correspond to the sum of a term of migration enthalpy and a term of interaction between the diffusing species and the segregated impurities.

4. Aluminium diffusion is faster than oxygen diffusion in both the lattice and the sub-boundaries.

5. Doping of alumina with Y_2O_3 induces an increase of lattice and sub-boundary diffusion but a decrease of grain boundary diffusion. In the lattice, it is due to the increase of "donor" impurity. In the sub-boundary, it is due to an increase in the dislocation density in the sub-boundaries, and the decrease of the intergranular diffusion is related to the yttrium segregation in the grain boundaries.

6. Calculations clearly indicate that the growth of alumina scales by oxidation of alumina former alloys is controlled by grain boundary or short-circuit diffusion. However, the short-circuits of scales must physically and chemically differ from those in massive alumina since the k_c values calculated from the fastest diffusion phenomenon are smaller than the experimental k_c values determined by oxidation experiments.

7. Yttrium should decrease the growth rate of alumina scales whatever the temperature (1100–1300°C).

8. Further experiments, particularly on aluminium grain-boundary diffusion, would be of great interest for a better understanding of the transport properties of alumina and for the interpretation of the growth mechanism of alumina scales.

Acknowledgements

The authors are indebted to D. Prot, whose results obtained for his thesis were used here for comparison, and to M. Miloche for her help in SIMS analyses at CNRS Bellevue.

References

1. A. M. HUNTZ, in "The role of Active Elements in the Oxidation Behaviour of High-temperature Metals and Alloys", edited by E. Lang (Elsevier Applied Science, London and New York, 1989) p. 81.
2. S. K. TIKU and F. A. KRÖGER, *J.Am. Ceram Soc.* **63** (1980) 31.
3. M. M. El-AIAT and F.A. KRÖGER, *ibid.* **65** (1982) 162.
4. H. A. WANG and F. A. KRÖGER, *ibid.* **63** (1980) 613.
5. F. A. KRÖGER, *Solid State Ionics* **12** (1984) 189.
6. M. LOUDJANI, B. LESAGE, G. PETOT-ERVAS, D. DEWERDEIR and A. M. HUNTZ, *Adv. Ceram.* **23** (1987) 125.
7. B. LESAGE, Doctorate Thesis, University of Paris XI (1984).
8. D. PROT, Thesis, University of Paris VI (1991).
9. M. K. LOUDJANI, Doctorate thesis, University of Paris XI (1992).
10. M. H. LAGRANGE, A. M. HUNTZ and J. Y. LAVAL, *Ann. Chim. Fr.* **12** (1987) 9.
11. K. KITAZAWA and R. L. COBLE, *J. Am. Ceram. Soc.* **57** (1974) 250.
12. M. DÉCHAMPS and F. BARBIER, in "Science of Ceramics Interfaces", edited by J. Nowotny (Elsevier Science, Amsterdam, 1991) 323.
13. M. K. LOUDJANI, A. M. HUNTZ and R. CORTÈS, *J. Mater. Sci.* **28** (1993) 6466.
14. K. P. R. REDDY, J. L. SMIALEK and A. R. COOPER, *Oxid. Met.* **17** (1982) 429.
15. E. W. A. YOUNG and J. H. W. DE WIT, *Solid State Ionics* **16** (1985) 39.
16. *Idem, Oxid. Met.* **26** (1986) 351.
17. A. E. PALADINO and W. D. KINGERY, *J. Chem Phys.* **37** (1962) 957.
18. Y. OISHI and W. D. KINGERY, *ibid.* **33** (1960) 480.
19. Y. OISHI, K. ANDO and Y. KUBOTA, *ibid.* **73** (1980) 1410.
20. Y. OISHI, K. ANDO, N. SUGA and W. D. KINGERY, *J. Am. Ceram. Soc.* **66** (1983) C 130.
21. D. J. REED and B. J. WUENCH, *ibid.* **63** (1980) 88.
22. K. P. R. REDDY and R. A. COOPER, *ibid.* **65** (1982) 634.
23. K. D. D. LAGERLOF, B. J. PLETKA, T. E. MITCHELL and A. H. HEUER, *Rad. Effects* **74** (1983) 87.
24. J. L. CADOZ, Doctorate Thesis, Université Paris XI (1978).
25. M. Le GALL, B. LESAGE and J. BERNARDINI, *Phil. Mag. A* (1994)
26. M. Le GALL, Doctorate thesis, University of Paris XI (1992).
27. M.Le GALL, B. LESAGE, A. M. HUNTZ and C. MONTY, *Phil. Mag. A* (1994)
28. A. D. Le CLAIRE and A. RABINOVITCH, *J. Phys. C, Solid State Phys.* **14** (1981) 3863.
29. B. LESAGE, Doctorate thesis, University of Paris XI (1984).
30. L. BADROUR, Doctorate thesis, University of Aix-Marseille III (1986).
31. D. PROT, M.MILOCHE and C. MONTY, *Coll. Physique C1* **51** *suppl.* (1990) 1027.
32. R. R. DILS, PhD thesis, Stanford University (1965).
33. G. J. DIENES, D. O. WELCH, C. F. FISHER, R. D. HATCHER, D. LAZARETH and M. SAMBERG, *Phys. Rev.* **B11** (1975) 3060.
34. M. K. LOUDJANI, A. M. HUNTZ, R. CORTÈS, *J. Mater. Sci.* **28** (1993) 6466.

35. M. K. LOUDJANI, Doctorate thesis, University of Paris XI (1992).
36. C. WAGNER, *Z. Phys. Chem. B.* (1933) 21.
37. J. NOWOK, *Oxid. Met.* **18** (1982) 1.
38. F. CLÉMENDOT, J. M. GRAS and J. C. VAN DUYSEN, in Proceedings of 3rd International Symposium on High Temperature Corrosion and Protection of Materials, Les Embiez, France, May 1992.
39. P. CHOQUET,C. INDRIGO and R. MEVREL, *Mater. Sci. Eng.* **88** (1987) 97.
40. P. CHOQUET, Doctorate thesis, University of Paris XI (1987).
41. J. JEDLINSKI, G. BORCHARDT and S. MROWEC, *Solid State Ionics* **50** (1992) 67.
42. D. N. CHAUBET, A. M. HUNTZ and F. MILLOT, *J. Mater. Sci.* **26** (1991) 6119.
43. A. C. S. SABIONI, A. M. HUNTZ, J. PHILIBERT, B. LESAGE and C. MONTY, *ibid.* **27** (1992) 4782.
44. A. ATKINSON, *Mater. Sci. Technol* **4** (1988) 1046.
45. F. BARBIER and M. DÉCHAMPS, *J. Physique, Coll. C5* **49** suppl. 10 (1988) 575.
46. F. BARBIER, C. MONTY and M. DÉCHAMPS, *Phil Mag.* **58** No. 3 (1988) 475.
47. A. M. HUNTZ, G. MOULIN and G. BEN ABDERRAZIK, *Ann. Chim. Fr.* **11** (1986) 291.
48. M. W. BRUMM and H. J. GRABKE, *Corr. Sci.* **33** (1992) 1677.
49. A. ATKINSON, *Rev. Mod. Phys.* **57** (1985) 437.

Received 6 September 1993
and accepted 9 June 1994